A Reproducing Kernel Hilbert Space Approach for Q-Ball Imaging

Enrico Kaden and Frithjof Kruggel*

***Abstract*—Diffusion magnetic resonance (MR) imaging has enabled us to reveal the white matter geometry in the living human brain. The Q-ball technique is widely used nowadays to recover the orientational heterogeneity of the intra-voxel fiber architecture. This article proposes to employ the Funk–Radon transform in a Hilbert space with a reproducing kernel derived from the spherical Laplace–Beltrami operator, thus generalizing previous approaches that assume a bandlimited diffusion signal. The function estimation problem is solved within a Tikhonov regularization framework, while a Gaussian process model allows for the selection of the smoothing parameter and the specification of confidence bands. Shortcomings of Q-ball imaging are discussed.**

***Index Terms*—Diffusion magnetic resonance (MR) imaging, Funk–Radon transform, Gaussian process model, Laplace–Beltrami operator, reproducing kernel Hilbert space.**

I. Introduction

THE white matter of the human brain consists of a complex system of nerve fibers that connect neural populations in the central nervous system. These long axons allow a rapid information exchange between distant brain modules, thereby integrating the diversity of cortical areas and subcortical nuclei with their specialized functional roles. Diffusion magnetic resonance (MR) imaging [1] is a unique tool to reveal the microgeometry of nervous tissue noninvasively and to explore the connectional neuroanatomy in the individual living human subject. This technique measures the Brownian dynamics of the spin-bearing water molecules in the underlying sample material. Depending on the direction from which the diffusion process is observed, the tissue geometry, especially the orientation of the axonal membranes, may hinder the diffusing molecules differently. If the examination period is sufficiently long and the fiber pathways are coherently oriented, the MR measurement exhibits anisotropic diffusion patterns.

A distinctive feature of white matter tissue is the orientational heterogeneity of the intra-voxel fiber architecture [2]. Since the fiber orientations are neither regularly ordered nor entirely arbitrary, it is interesting to know how the tangents at the fiber pathways are oriented. This knowledge is necessary to reconstruct the course of the fiber tracts and to estimate the structural connectivity of different brain regions. Until now, the connectional architecture of the cerebral cortex is still far from being known in full detail even at the systems level, not least due to the anatomical variability between subjects. Q-ball imaging [3], which is one of the methods that is most widely used nowadays, attempts to obtain information about the orientational structure in a voxel from diffusion-weighted measurements. This approach is implemented without the specification of a forward-generative model that maps the geometry of nervous tissue onto the diffusion process of water molecules and further onto the observable MR signal. The simple idea is to approximate the orientation density function of the diffusion propagator by integrating the diffusion signal with a fixed b-value over the equator normal to the direction under consideration. This neuroimaging technique is particularly applicable in the clinical domain due to a short acquisition time. Recent methodological developments include the introduction of the solid angle into the definition of the orientation density function, assuming a (local) exponential decay along all gradient directions (and a finite signal support, respectively) [4]–[7]. However, these transforms of the diffusion signal do not longer fulfil the superposition property. Khachaturian *et al.* [8] presented a technique for multiple b-values, which requires a longer data acquisition, and Deriche *et al.* [9] proposed a real-time recovery algorithm within a Kalman filtering framework. For a review of alternative reconstruction methodologies see, for example, [10] and references therein.

Our main objective is to develop a novel computational method for the nonparametric estimation of the diffusion signal and the orientation density function (as defined by Q-ball imaging). To that end, we revisit the statistical problem of estimating an unknown function, which is defined on the two-dimensional sphere, from a finite set of noisy MR observations. The key question is here in which function space this variational problem should be solved. Previous work [11]–[13] suggested to truncate the Fourier decomposition of the square-integrable functions on the sphere, thereby cutting off the high frequency components. But is the truncation step necessary for the estimation of the diffusion signal? We will show that it is indeed possible to relax this assumption. More specifically, we assume rather general conditions about the integrability and the regularity of the spherical functions to be estimated, which give rise to a reproducing kernel Hilbert space that is infinite-dimensional but computationally manageable. Considering generic functions being less constrained by our prior belief enlarges the solution space, lets the data speak

Manuscript received March 17, 2011; revised May 03, 2011; accepted May 10, 2011. Date of publication May 23, 2011; date of current version November 02, 2011. *Asterisk indicates corresponding author.*

E. Kaden is with the Department of Computer Science, University of Leipzig, Johannisgasse 26, 04103 Leipzig, Germany (e-mail: enrico.kaden@gmail.com).

*F. Kruggel is with the Department of Biomedical Engineering, University of California, Irvine, Irvine, CA 92697 USA (e-mail: fkruggel@uci.edu).

Color versions of one or more of the figures in this paper are available online at http://ieeexplore.ieee.org.

Digital Object Identifier 10.1109/TMI.2011.2157517

for themselves, and thus generates better evidence. Another important aim of this work is to estimate rigorously all hyperparameters (e.g., the signal smoothness and the noise variance, yielding the smoothing parameter) from the data or, if possible, to avoid them completely (e.g., the truncation level if we do not truncate the Fourier series expansion). Note that these parameters significantly affect the nonparametric function estimation. For example, if the smoothing parameter approaches infinity, the estimate is a constant function on the sphere. If this hyperparameter is set to zero, the measurement noise appears to be a part of the signal. Moreover, we propose several improvements to Q-ball imaging: The MR signal without any diffusion weighting (i.e., the T_2-contrast) is integrated into the regularization problem. We pay attention to the noise variance modifications due to linear interpolation required for the correction of subject motion and the co-registration with an anatomical coordinate system. Further, the reproducing kernel (with antipodal symmetry), which is derived from the spherical Laplace–Beltrami operator, as well as the Funk–Radon transform of this kernel function are given for the first time in a closed-form expression.

The following section presents the nonparametric function estimation of the diffusion signal using a smoothing spline model. For this purpose we make the vague assumption that the signal is a suitably smooth function on the sphere whose harmonic coefficients decay sufficiently fast. After revisiting the Q-ball imaging formalism, the orientation density function of the diffusion propagator is approximated by the Funk–Radon transform of the diffusion signal, which is represented in a reproducing kernel Hilbert space. Furthermore, we formulate a Gaussian process model that defines a probability measure on this function space. The Bayesian paradigm enables the specification of confidence bands and the setting of the smoothing parameter, which is decomposed into the roughness of the diffusion signal and the noise variance of the MR measurement. Next, we discuss results from a simulation study and exemplify the statistical estimation of the orientation density function in various brain regions, using a diffusion-weighted dataset featuring high angular resolution. We conclude with a discussion of the limitations of Q-ball imaging.

II. Theory and Methods

A. Nonparametric Signal Estimation

Consider a pulsed gradient spin echo experiment in which the temporal profile of the diffusion sensitizing gradients and their magnitude $|G|$ are fixed, but the (normalized) direction $g = G/|G|$ is variable. Let $\boldsymbol{y}$ be n noisy MR observations $y^{(i)} = E_b(g^{(i)}) + \varepsilon^{(i)}$ at each site for the design points $\boldsymbol{x} = \{g^{(i)} \in S^2 : i = 1, \ldots, n\}$ with pairwise different $\pm g^{(i)}$. b denotes the constant diffusion weighting factor, which is calculated from $|G|$ and the temporal profile of the diffusion encoding gradients, and $\varepsilon^{(i)} \sim \mathcal{N}(0, w^{(i)}\sigma^2)$ describes the Gaussian-distributed noise with unknown variance σ^2. The factor $w^{(i)}$ represents the noise variance modification caused by the linear interpolation owing to the correction for subject motion and the co-registration with an anatomical coordinate system [14]. The diffusion signal $e_b(g) = E_b(g)/E_0$ should not depend on the attenuation due to the T_2-relaxation process, where E_0 denotes the MR signal in the absence of any diffusion weighting. Given the sample mean $\hat{E}_0$ of the signal with zero b-value, the Tikhonov regularization framework estimates the diffusion signal $\hat{e}_b$ via a smoothing spline model [15] that minimizes

$$I_\xi(e_b) = \sum_{i=1}^{n} \frac{1}{w^{(i)}} \left(y^{(i)} - \hat{E}_0 e_b\left(g^{(i)}\right)\right)^2 + \xi \int_{S^2} |\Delta e_b(g)|^2 \, dg \tag{1}$$

with respect to the observed MR signals (compare also [13]). This variational problem depends on the appropriately chosen parameter $\xi \geq 0$ balancing the smoothness of the solution (as $\xi \to \infty$) against the fidelity to the data (as $\xi \to 0$).

The Laplace–Beltrami operator $\Delta : L^2(S^2) \supset H \to L^2(S^2)$ is a linear map from a function space H, which we will give below, to the real-valued square-integrable functions $L^2(S^2)$ on the sphere that is defined by

$$\Delta = -\left(\frac{1}{\sin\theta} \frac{\partial}{\partial\theta} \left(\sin\theta \frac{\partial}{\partial\theta} \right) + \frac{1}{\sin^2\theta} \frac{\partial^2}{\partial\phi^2} \right) \tag{2}$$

in the polar coordinates $\theta \in [0, \pi)$ and $\phi \in [0, 2\pi)$. The eigenvalues of this differential operator are $\lambda_{l,m} = l(l+1)$ for $-l \leq m \leq l$ and $l = 0, 1, \ldots$; the corresponding eigenfunctions, i.e., the real L^2-normalized spherical harmonics

$$Y_{l,m}(\theta,\phi) = \begin{cases} \sqrt{2}\sqrt{\frac{2l+1}{4\pi}\frac{(l-m)!}{(l+m)!}} & \\ \quad \times P_{l,m}(\cos\theta)\cos(m\phi), & \text{if } m > 0 \\ \sqrt{\frac{2l+1}{4\pi}} P_l(\cos\theta), & \text{if } m = 0 \\ \sqrt{2}\sqrt{\frac{2l+1}{4\pi}\frac{(l-|m|)!}{(l+|m|)!}} & \\ \quad \times P_{l,|m|}(\cos\theta)\sin(|m|\phi), & \text{if } m < 0 \end{cases} \tag{3}$$

form an orthonormal basis representing a Fourier decomposition of $L^2(S^2)$ [16]. The Legendre polynomials $P_{l,m}(s)$ are defined by $P_{l,m}(s) = (-1)^m (1-s^2)^{m/2} d^m/ds^m P_l(s)$ for $m \geq 0$ and otherwise $P_{l,m}(s) = (-1)^{|m|}(l-|m|)!/(l+|m|)! P_{l,|m|}(s)$ with

$$P_l(s) = \frac{1}{2^l l!} \frac{d^l}{ds^l}(s^2-1)^l \tag{4}$$

on the interval $[-1, 1]$. Note that the nonnegative eigenvalues do not have an upper bound.

Before proceeding, we give a brief introduction to reproducing kernel Hilbert spaces [17]. Let H be a Hilbert space (i.e., a complete normed space with an inner product $\langle \cdot, \cdot \rangle_H$) which consists of real-valued functions defined on a set, here S^2. A *reproducing kernel* for H is a function $\zeta : S^2 \times S^2 \to \mathbb{R}$ with the following properties. 1) For all $\omega \in S^2$, $\zeta(\cdot, \omega)$ as univariate function belongs to H. 2) The evaluation of a function $f \in H$ at a point $\omega \in S^2$ can be rewritten as

$$f(\omega) = \langle f, \zeta(\cdot, \omega) \rangle_H . \tag{5}$$

If such a reproducing kernel exists in H, then this kernel function is uniquely defined. Consider the linear map $\mathrm{ev}_\omega : H \to \mathbb{R}$ with $f \mapsto f(\omega)$ that evaluates a function $f \in H$ at a point $\omega \in S^2$. This evaluation functional ev_ω is continuous if and only if there exists an $M \geq 0$ with $\|\mathrm{ev}_\omega f\| \leq M \|f\|_H$ for all

$f \in H$. Since there exists a reproducing kernel for H if and only if all functionals $f \mapsto f(\omega)$, $\omega \in S^2$ are continuous in H, we arrive at the following definition [17]: A *reproducing kernel Hilbert space* is a Hilbert space of functions such that all evaluation functionals are linear and continuous. If H is a finite-dimensional Hilbert space, then ev_ω is continuous and H is thus a Hilbert space with reproducing kernel. If the function space H is not finite-dimensional, then ev_ω may or may not be continuous.

Next, we define the function space $H \subset L^2(S^2)$ in which the regularization problem (1) is solved. The diffusion signal e_b is assumed to be a real-valued function with the property $e_b(g) = e_b(-g)$, $g \in S^2$ (antipodal symmetry). Further, we make the assumption that all evaluation functionals $\mathrm{ev}_g : H \to \mathbb{R}$ with $e_b \mapsto e_b(g)$ are linear and continuous, where $g \in S^2$ denotes the gradient direction and b specifies the diffusion weighting factor. Then H is a Hilbert space with reproducing kernel, which means that for each $g \in S^2$ there exists a unique $\zeta(\cdot, g) \in H$ with $\mathrm{ev}_g e_b = e_b(g) = \langle e_b, \zeta(\cdot, g)\rangle_H$. In this work we derive the reproducing kernel $\zeta : S^2 \times S^2 \to \mathbb{R}$ from the Laplace–Beltrami operator on the sphere, yielding the separable SO(3)-Hilbert space $H = H^0 \oplus H^1$ formed by the direct sum of

$$H^0 = \left\{ e_b^0 = e_{0,0} Y_{0,0} \in L^2(S^2) : \left\| e_b^0 \right\|_{H^0}^2 = |e_{0,0}|^2 < \infty \right\} \tag{6}$$

and

$$H^1 = \left\{ e_b^1 = \sum_{\substack{l=2,\\ l \text{ even}}}^{\infty} \sum_{m=-l}^{l} e_{l,m} Y_{l,m} \in L^2(S^2) : \left\| e_b^1 \right\|_{H^1}^2 = \sum_{\substack{l=2,\\ l \text{ even}}}^{\infty} \sum_{m=-l}^{l} \left(l(l+1)\right)^2 |e_{l,m}|^2 < \infty \right\} \tag{7}$$

whose harmonic coefficients $e_{l,m} = \int_{S^2} e_b(g) Y_{l,m}(g) dg$ decay sufficiently fast. In comparison, previous methods [11]–[13] truncate the spherical harmonic expansion. Note that due to the antipodal symmetry, we need to take only coefficients with even l into account. The reproducing kernel for H writes $\zeta(\omega, \psi) = \zeta^0(\omega, \psi) + \zeta^1(\omega, \psi)$ with

$$\zeta^0(\omega, \psi) = \frac{1}{4\pi} \tag{8}$$

and

$$\begin{aligned} \zeta^1(\omega, \psi) &= \sum_{\substack{l=2,\\ l \text{ even}}}^{\infty} \sum_{m=-l}^{l} \frac{1}{\left(l(l+1)\right)^2} Y_{l,m}(\omega) Y_{l,m}(\psi) \\ &= \frac{1}{4\pi} \sum_{\substack{l=2,\\ l \text{ even}}}^{\infty} \frac{2l+1}{\left(l(l+1)\right)^2} P_l\left(\langle \omega, \psi \rangle\right) \end{aligned} \tag{9}$$

which can be simplified to

$$\zeta^1(\omega, \psi) = \frac{1}{8\pi} \left(2 - \frac{\pi^2}{6} - \ln\left(\frac{1 + \langle \omega, \psi \rangle}{2} \right) \cdot \ln\left(\frac{1 - \langle \omega, \psi \rangle}{2} \right) \right) \tag{10}$$

[18]. Even though the latter equation is not defined for $\langle \omega, \psi \rangle = \pm 1$, we have $\lim_{s \to \pm 1} 1/(8\pi)(2 - \pi^2/6 - \ln((1+s)/2)\ln((1-s)/2)) = 1/(8\pi)(2 - \pi^2/6)$ as expected. In particular, the second-order differential operator $\Delta : L^2(S^2) \supset H \to L^2(S^2)$ with

$$\begin{aligned} e_b &= \sum_{\substack{l=0,\\ l \text{ even}}}^{\infty} \sum_{m=-l}^{l} e_{l,m} Y_{l,m} \mapsto \\ \Delta e_b &= \sum_{\substack{l=0,\\ l \text{ even}}}^{\infty} \sum_{m=-l}^{l} l(l+1) e_{l,m} Y_{l,m} \end{aligned} \tag{11}$$

is well defined. The diffusion signal $e_b = e_b^0 + e_b^1 \in H$ is uniquely decomposed into a constant function $e_b^0 \in H^0$ and a variable part $e_b^1 \in H^1$, where

$$\begin{aligned} \left\| e_b^1 \right\|_{H^1}^2 &= \sum_{\substack{l=2,\\ l \text{ even}}}^{\infty} \sum_{m=-l}^{l} \left(l(l+1)\right)^2 |e_{l,m}|^2 \\ &= \int_{S^2} |\Delta e_b|^2 dg = \|\Delta e_b\|_{L^2}^2 \end{aligned} \tag{12}$$

quantifies the roughness of the unknown function in terms of the spherical Laplace–Beltrami operator. Hence, the regularization term in the smoothing spline model (1) can be reformulated using the subspace norm $\| \cdot \|_{H^1}$.

According to the representation theorem by Kimeldorf and Wahba [19], there exists a unique solution $\hat{e}_b \in H$ for the penalized least squares problem (1), which may be represented by $\hat{e}_b = \hat{e}_b^0 + \hat{e}_b^1$ with

$$\hat{e}_b^0(g) = \alpha Y_{0,0} \in H^0 \quad \text{and} \quad \hat{e}_b^1(g) = \sum_{i=1}^{n} \beta_i \zeta^1\left(g, g^{(i)}\right) \in H^1 \tag{13}$$

for all $g \in S^2$ in terms of the scalar $\alpha \in \mathbb{R}$ and the real-valued n-vector $\boldsymbol{\beta}$. Note that for $1 \leq n < \infty$ MR observations the estimated diffusion signal can be written as a finite sum, although e_b generally lies in the infinite-dimensional function space H. The signal in adjacent voxels is implicitly supposed to be independent. Setting this representation of $\hat{e}_b$ into the quadratic objective function (1), we obtain

$$\alpha = \left(J^t \left[K + \xi / \hat{E}_0^2 W \right]^{-1} J \right)^{-1} J^t \left[K + \xi / \hat{E}_0^2 W \right]^{-1} \boldsymbol{y} / \hat{E}_0 \tag{14}$$

and

$$\boldsymbol{\beta} = \left[K + \xi / \hat{E}_0^2 W \right]^{-1} \left\{ I_n - J \left(J^t \left[K + \xi / \hat{E}_0^2 W \right]^{-1} J \right)^{-1} \times J^t \left[K + \xi / \hat{E}_0^2 W \right]^{-1} \right\} \boldsymbol{y} / \hat{E}_0 \tag{15}$$

where $\boldsymbol{y}$ denotes the n-vector $(y^{(i)})_i$, J is the n-vector $(Y_{0,0})_i$, K forms the $n \times n$-matrix $(\zeta^1(g^{(i)}, g^{(j)}))_{i,j}$ as defined in (10), I_n is the n-dimensional unit matrix, and W denotes the n-dimensional diagonal matrix with the entries $(w^{(i)})_{i,i}$. An equivalent representation of the solution to this variational problem

takes the form

$$J\alpha + \left(K + \xi/\hat{E}_0^2 W\right)\boldsymbol{\beta} = \boldsymbol{y}/\hat{E}_0 \quad \text{subject to} \quad J^t\boldsymbol{\beta} = 0 \tag{16}$$

which may be found more convenient for numerical computation. The minimization problem is linear in α and $\boldsymbol{\beta}$.

Nonparametric Bayesian statistics provides an inferential framework for statistical modeling and analysis, enabling the differentiation between relevant features of the diffusion signal and artifacts due to the measurement noise. We exploit the close relationship between smoothing splines and Gaussian process models [20]. The prior knowledge about the signal function e_b may be encoded by a Gaussian stochastic process

$$e_b|M, \alpha \sim \mathcal{GP}(m_{\text{prior}}, k_{\text{prior}}) \tag{17}$$

with the mean function $m_{\text{prior}}(g) = \alpha Y_{0,0}$, $\alpha \sim \mathcal{N}(m_\alpha, \sigma_\alpha^2)$ and the covariance function $k_{\text{prior}}(\omega, \psi) = \tau^2\zeta^1(\omega, \psi)$, where $\tau^2 \geq 0$ is a scaling parameter and M describes the model hyperparameters. Integrating out the prior distribution on the hyperparameter α, the prior Gaussian process can be reformulated as

$$e_b|M, m_\alpha, \sigma_\alpha^2 \sim \mathcal{GP}\left(m_\alpha Y_{0,0}, \tau^2\zeta^1(\omega, \psi) + \sigma_\alpha^2/(4\pi)\right) \tag{18}$$

[21]. The likelihood function updates this prior process by extracting the hidden information about e_b from the noisy MR signals $\boldsymbol{y}$ at the design points $\boldsymbol{x}$. According to Bayes' theorem, we obtain the posterior Gaussian process

$$e_b|\boldsymbol{y}, \boldsymbol{x}, E_0, M, m_\alpha, \sigma_\alpha^2 \sim \mathcal{GP}(m_{\text{post}}, k_{\text{post}}) \tag{19}$$

[22]. To establish the correspondence with the Tikhonov regularization framework proposed above, the prior distribution of α is assumed to be noninformative, i.e., $\sigma_\alpha^2 \to \infty$ (m_α irrelevant). Then the mean function m_{post} of the posterior Gaussian process equals the smoothing spline solution. The posterior covariance function writes

$$\begin{aligned} k_{\text{post}}(\omega, \psi) = k_{\text{prior}}(\omega, \psi) - U(\omega)^t \left[\tau^2 K + \sigma^2/E_0^2 W\right]^{-1} U(\psi) \\ + V(\omega)^t \left(J^t \left[\tau^2 K + \sigma^2/E_0^2 W\right]^{-1} J\right)^{-1} V(\psi) \end{aligned} \tag{20}$$

where $U(\cdot)$ denotes the n-vector $(\tau^2\zeta^1(\cdot, g^{(i)}))_i$ and $V(\cdot) = Y_{0,0} - J^t[\tau^2 K + \sigma^2/E_0^2 W]^{-1}U(\cdot)$ is a one-dimensional vector function.

Thus far, we have assumed that $M = \{\tau^2, \sigma^2\}$ is known, which is typically not the case. To determine the hyperparameters M that best explain the observed phenomenon, the density function $f(\boldsymbol{y}; \tau^2, \sigma^2; \sigma_\alpha^2)$ of the marginal distribution

$$\begin{aligned} \boldsymbol{y}|\boldsymbol{x}, E_0, M, m_\alpha, \sigma_\alpha^2 \\ \sim \mathcal{N}\left(E_0 J m_\alpha, E_0^2\tau^2 K + \sigma^2 W + E_0^2\sigma_\alpha^2 J J^t\right) \end{aligned} \tag{21}$$

is maximized, which is, however, not appropriate in the limiting case $\sigma_\alpha^2 \to \infty$. Recall that E_0 denotes the MR signal in the absence of any diffusion weighting, J is the n-vector $(Y_{0,0})_i$, K forms the $n \times n$-matrix $(\zeta^1(g^{(i)}, g^{(j)}))_{i,j}$ as defined in (10), and W denotes the n-dimensional diagonal matrix with the noise variance modifications $(w^{(i)})_{i,i}$. Consider the QR decomposition $J = (Q_1\ Q_2)(R^t\ 0^t)^t$ with the $n \times 1$-matrix Q_1 and the $n \times (n-1)$-matrix Q_2, where $Q = (Q_1\ Q_2)$ is orthogonal and R denotes an upper triangular matrix. Setting $\boldsymbol{z} = Q_2^t\boldsymbol{y}$ and noting that $Q_2^t J = 0$, we maximize the density $g(\boldsymbol{z}; \tau^2, \sigma^2)$ of the normal distribution

$$\boldsymbol{z}|\boldsymbol{x}, E_0, M \sim \mathcal{N}\left(0, E_0^2\tau^2 Q_2^t K Q_2 + \sigma^2 Q_2^t W Q_2\right) \tag{22}$$

with respect to M. For a constant $C > 0$ independent of τ^2 and σ^2 it can be shown that

$$g(\boldsymbol{z}; \tau^2, \sigma^2) = C \lim_{\sigma_\alpha^2 \to \infty} \left(\sigma_\alpha^2\right)^{1/2} f\left(\boldsymbol{y}; \tau^2, \sigma^2; \sigma_\alpha^2\right) \tag{23}$$

where f is normalized by $(\sigma_\alpha^2)^{1/2}$ to avoid degeneracy [23]. The regularization parameter $\xi = \sigma^2/\tau^2$ is composed of the noise variance $\sigma^2 \geq 0$ of the MR measurement and the scaling parameter $\tau^2 \geq 0$ of the prior covariance function controlling the smoothness of the diffusion signal.

B. Q-Ball Imaging

Let $\boldsymbol{r} = R\omega \in \mathbb{R}^3$ denote the relative displacement of a water molecule in spherical coordinates where $R \in [0, \infty)$ is the radius and $\omega \in S^2$ the direction. Q-ball imaging [3] attempts to approximate the orientation density function (i.e., the radial projection that is defined without the Jacobian R^2 of the transformation from Cartesian to spherical coordinates)

$$\varphi(\omega) = \frac{1}{C_\varphi} \int_0^\infty p_t(R\omega) dR \tag{24}$$

of the ensemble-averaged diffusion propagator p_t with the observation time t using the Funk–Radon transform

$$\phi(\omega) = \frac{1}{C_\phi} \int_{\omega^\perp} e_b(g) dg \tag{25}$$

of the diffusion signal e_b with a fixed b-value. $\omega^\perp = \{\psi \in S^2 : \langle\omega, \psi\rangle = 0\}$ denotes the equator normal to the direction $\omega \in S^2$. C_φ and C_ϕ are normalization constants such that these functions integrate to one over the sphere.

First, we neglect the normalization factor. Since it holds $\int_{\omega^\perp} Y_{l,m}(\chi) d\chi = 2\pi P_l(0) Y_{l,m}(\omega)$ [12], [13], the Funk–Radon transform of the reproducing kernel (10) writes

$$\begin{aligned} \eta^1(\omega, \psi) &= \int_{\omega^\perp} \zeta^1(\chi, \psi) d\chi \\ &= \frac{1}{2} \sum_{\substack{l=2, \\ l \text{ even}}}^\infty \frac{2l+1}{(l(l+1))^2} P_l(0) P_l\left(\langle\omega, \psi\rangle\right) \end{aligned} \tag{26}$$

which can be simplified to

$$\begin{aligned} \eta^1(\omega, \psi) = \frac{1}{2}\left(1 - \frac{\pi^2}{12} - \frac{\ln(2)^2}{2} + \ln(2)\ln\left(\frac{1 + |\langle\omega, \psi\rangle|}{2}\right)\right. \\ \left. + \text{Li}_2\left(\frac{1 - |\langle\omega, \psi\rangle|}{2}\right)\right) \end{aligned} \tag{27}$$

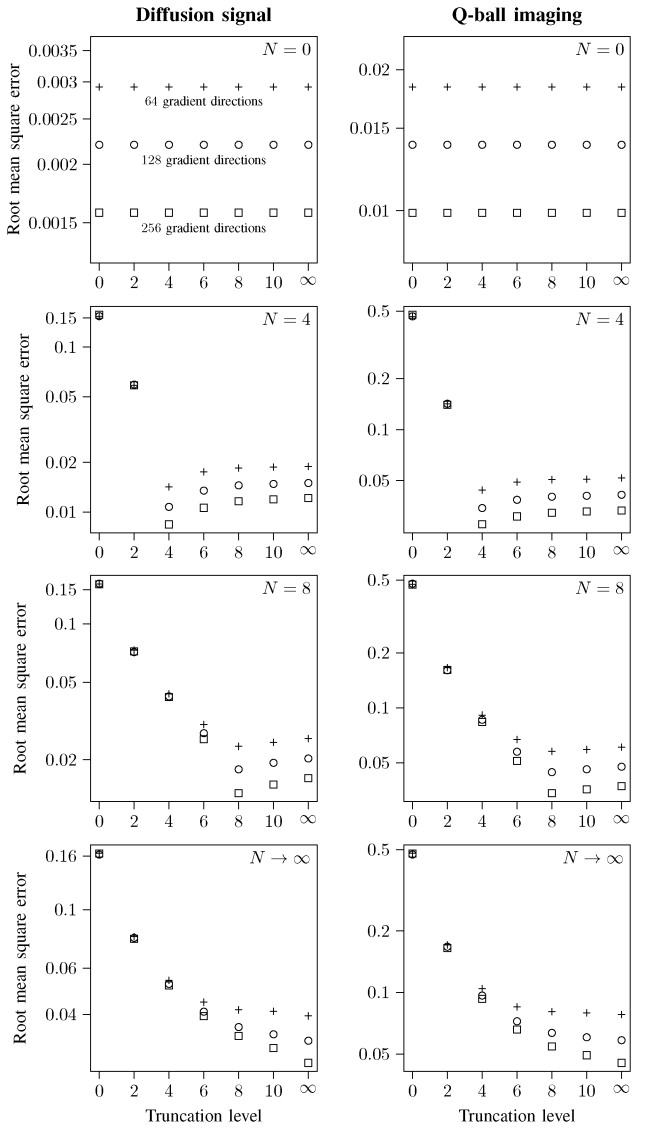

Fig. 1. This simulation study compares the estimation error of the diffusion signal (left) and the orientation density function with respect to the truncation level of the spherical harmonic expansion for different numbers of gradient directions. The sample mean of the root mean square error is shown for synthetic signals simulated with different truncations n (indicated in the upper right corner of the diagrams), where $N \to \infty$ corresponds to the reproducing kernel Hilbert space approach.

[18]. $\mathrm{Li}_2(s)$ denotes the dilogarithm for $s \in [-1, 1]$. Assuming that $\hat{e}_b$ is represented by (13), the orientation density function may be described by $\hat{\phi} = \hat{\phi}^0 + \hat{\phi}^1$ with

$$\hat{\phi}^0(\omega) = \alpha\sqrt{\pi} \quad \text{and} \quad \hat{\phi}^1(\omega) = \sum_{i=1}^{n} \beta_i \eta^1\left(\omega, g^{(i)}\right) \tag{28}$$

for all $\omega \in S^2$ in terms of the scalar $\alpha \in \mathbb{R}$ and the real-valued n-vector $\boldsymbol{\beta}$. Note that the Funk–Radon transform is a continuous linear operator in the Hilbert space H. Again, we exploit the correspondence between the smoothing spline solution and the posterior Gaussian process $\phi|\boldsymbol{y}, \boldsymbol{x}, E_0, M, m_\alpha, \sigma_\alpha^2 \sim \mathcal{GP}(m_{\mathrm{post}}, k_{\mathrm{post}})$, assuming that the prior distribution of α is noninformative, i.e., $\sigma_\alpha^2 \to \infty$ (m_α irrelevant). Then the mean function m_{post} equals $\hat{\phi}$. The posterior covariance function takes the form

$$\begin{aligned} k_{\mathrm{post}}(\omega, \psi) = {} & \tau^2 \theta^1(\omega, \psi) - U(\omega)^t \left[\tau^2 K + \sigma^2 / E_0^2 W\right]^{-1} U(\psi) \\ & + V(\omega)^t \left(J^t \left[\tau^2 K + \sigma^2 / E_0^2 W\right]^{-1} J\right)^{-1} V(\psi) \end{aligned} \tag{29}$$

where $U(\cdot)$ denotes the n-vector $(\tau^2 \eta^1(\cdot, g^{(i)}))_i$, $V(\cdot) = \sqrt{\pi} - J^t[\tau^2 K + \sigma^2/E_0^2 W]^{-1} U(\cdot)$ is a one-dimensional vector function, and

$$\begin{aligned} \theta^1(\omega, \psi) &= \int_{\omega^\perp} \int_{\psi^\perp} \zeta^1(\chi, \chi') d\chi d\chi' \\ &= \pi \sum_{\substack{l=2, \\ l \text{ even}}}^{\infty} \frac{2l+1}{(l(l+1))^2} P_l(0)^2 P_l(\langle \omega, \psi \rangle). \end{aligned} \tag{30}$$

Finally, the normalization constant is computed by $C_\phi = 4\pi^{3/2}\alpha$.

C. Data Acquisition and Preprocessing

The diffusion-weighted MR dataset, which was kindly provided by the 2009 Pittsburgh Brain Connectivity Competition[1] [24], online available at , was acquired by a 3T Magnetom Trio scanner (Siemens, Erlangen) equipped with a 32-channel phased-array head coil. A spin echo EPI sequence measured 256 diffusion gradient directions with a b-value of 1500 $\mathrm{s/mm^2}$. These directions and their antipodal points were uniformly distributed on the sphere. Further, 30 images without diffusion weighting were acquired. The sequence timing with an echo time $t_{\mathrm{TE}} = 108$ ms and the repetition time $t_{\mathrm{TR}} = 11.6$ s was fixed in this MR experiment. The diffusion images were reconstructed by a 6/8 partial Fourier encoding scheme. The measurement of 68 slices with 2 mm thickness (no slice gap) and a 128 × 128 image matrix (with a field of view 256 × 256 $\mathrm{mm^2}$) covered the whole brain, resulting in an acquisition time of about 55 min. A male volunteer (aged 27 years) participated in this study. The dataset was corrected for subject motion with respect to the images having a b-value of 0 $\mathrm{s/mm^2}$ and co-registered with a T_1-weighted MR volume using rigid-body transformations [25], as implemented in FSL [26]. For this purpose the diffusion-weighted images, which have an isotropic voxel resolution of 2 mm, were resampled by linear interpolation. As a consequence, the noise variance is modified by the factor

$$w(x, y, z) = \sum_{i,j,k \in \mathbb{Z}} \Lambda(x/T - i)^2 \Lambda(y/T - j)^2 \Lambda(z/T - k)^2 \tag{31}$$

at the location $(x, y, z) \in \mathbb{R}^3$, assuming that the original dataset is spatially uncorrelated [14]. T is the step size of the uniform sampling, $\Lambda(s)$ denotes the hat function with $\Lambda(s) = 1 - |s|$ for $|s| \leq 1$ and $\Lambda(s) = 0$ otherwise. The T_1-weighted anatomical dataset was aligned with the stereotactic coordinate system [27] without spatial normalization.

[1]Available online at http://www.braincompetition.org.

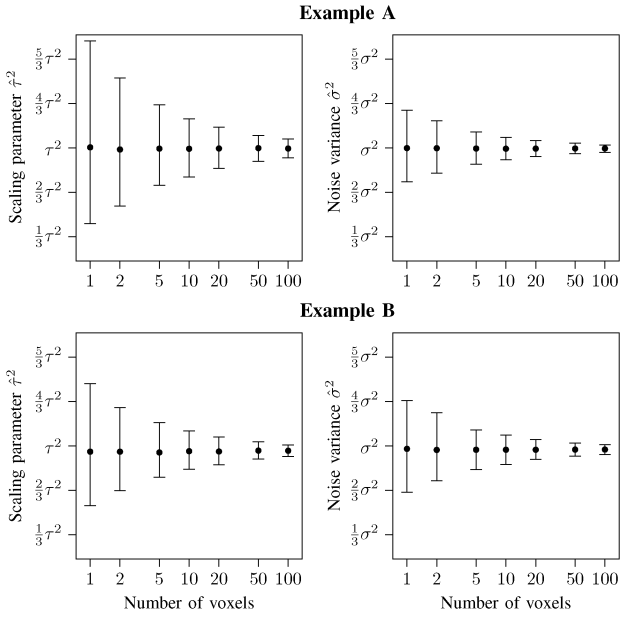

Fig. 2. The diagrams show for two examples the sample mean including the 95% confidence interval for the estimation of the scaling parameter $\hat{\tau}^2$ and the noise variance $\hat{\sigma}^2$ with respect to the number of voxels, which was repeated 1000 times. The quantities without hat, i.e., τ^2 and σ^2, denote the true value. See text for further details on this simulation study.

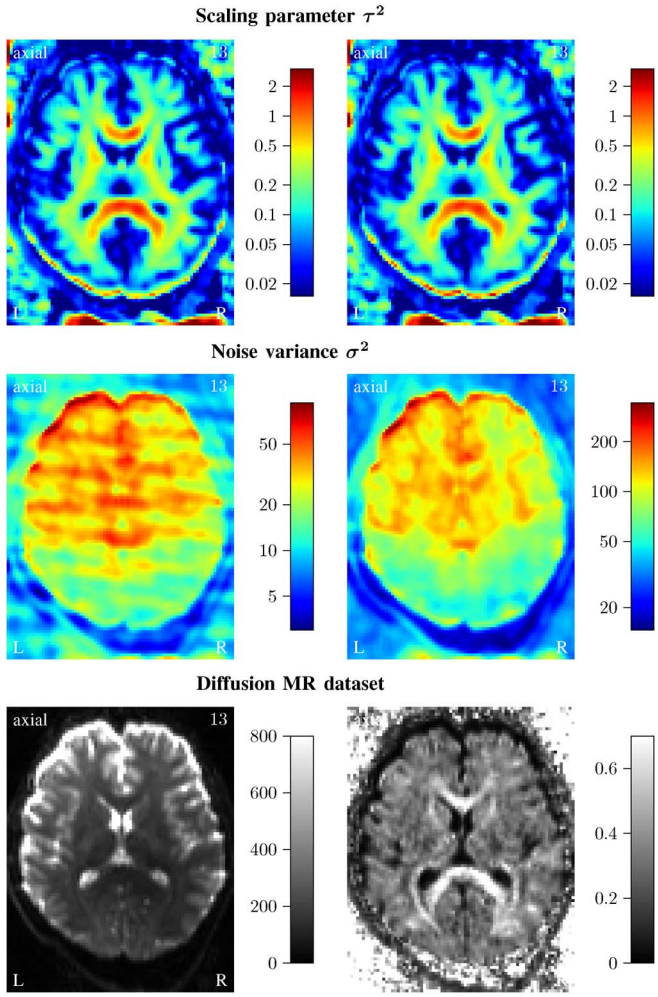

Fig. 3. The first two rows illustrate the estimation of the scaling parameter τ^2 (top) and the noise variance σ^2 in the 26-neighborhood of a voxel. On the left-hand side the variance modifications due to the linear interpolation are neglected, whereas in the right section the modification factor is taken into account. The bottom row exemplifies an MR image without any diffusion weighting (left) and the diffusion signal for one of the gradient directions with a b-value of $1500\mathrm{s}/\mathrm{mm}^2$.

III. Results

A. Simulations

First, we compare the estimation error of the diffusion signal and the orientation density function between a previous reconstruction method which truncates the spherical harmonic expansion [13] and the reproducing kernel Hilbert space approach proposed in this work. The signal is simulated using different signal models where the Fourier decomposition is truncated at the levels $N = 0$, 4, 8, and $N \to \infty$ (no truncation). If $N < \infty$, then the Fourier coefficients $e_{l,m}$ with $-l \leq m \leq l$ and $l \leq N$ are drawn from a normal distribution whose variance is weighted by $1/(l(l+1))^2$, with the exception of $e_{0,0}$ which is fixed. In the case of no truncation $(N \to \infty)$, the Gaussian process model generates the synthetic signals. We run 1000 trials for each signal model to simulate MR measurements for 64, 128, and 256 gradient directions that are disturbed by Rician noise. In an effort to make the results from different algorithms comparable, the smoothing parameter ξ, which has to be user-defined in [13], is selected by an oracle estimator which minimizes the predictive mean square error. The computation time depends on the chosen truncation N: If $(N+1)(N+2)/2$ is smaller than the number of measurements n, then the previous reconstruction methods which cut off the high frequency components are faster. In the case of $(N+1)(N+2)/2 > n$ with a spatially dependent regularization parameter, the reproducing kernel Hilbert space approach requires less computation time. Fig. 1 shows the sample mean of the root mean square error between the original and the recovered diffusion signal (left) and orientation density function with respect to the truncation level of the applied algorithm. This simulation study suggests that if the signal model is known, the recovery method with the same truncation level yields the smallest estimation error. If the signal complexity is underestimated, i.e., n is chosen too small, then the root mean square error is rather high. Even if more and more data are acquired, that is, the number of gradient directions approaches infinity, the estimation error cannot be smaller than a certain threshold greater than zero. Further, Fig. 1 demonstrates that if the truncation level n of the reconstruction algorithm is greater than the signal complexity, then the root mean square error is higher than the optimal one, but only slightly. Note that a log scale is used to depict the estimation error in these diagrams. Since it is commonly unknown whether the Fourier decomposition of the observed signal is truncated, the reproducing kernel Hilbert space approach seems to be the better strategy for the statistical estimation of the diffusion signal and the orientation density function: On average, the root mean square error is minimized in the case of no truncation, or the estimation error is slightly increased, but significantly smaller than the resulting error if the truncation level is underestimated.

The accurate determination of the hyperparameters (i.e., the scaling parameter τ^2 of the prior covariance function

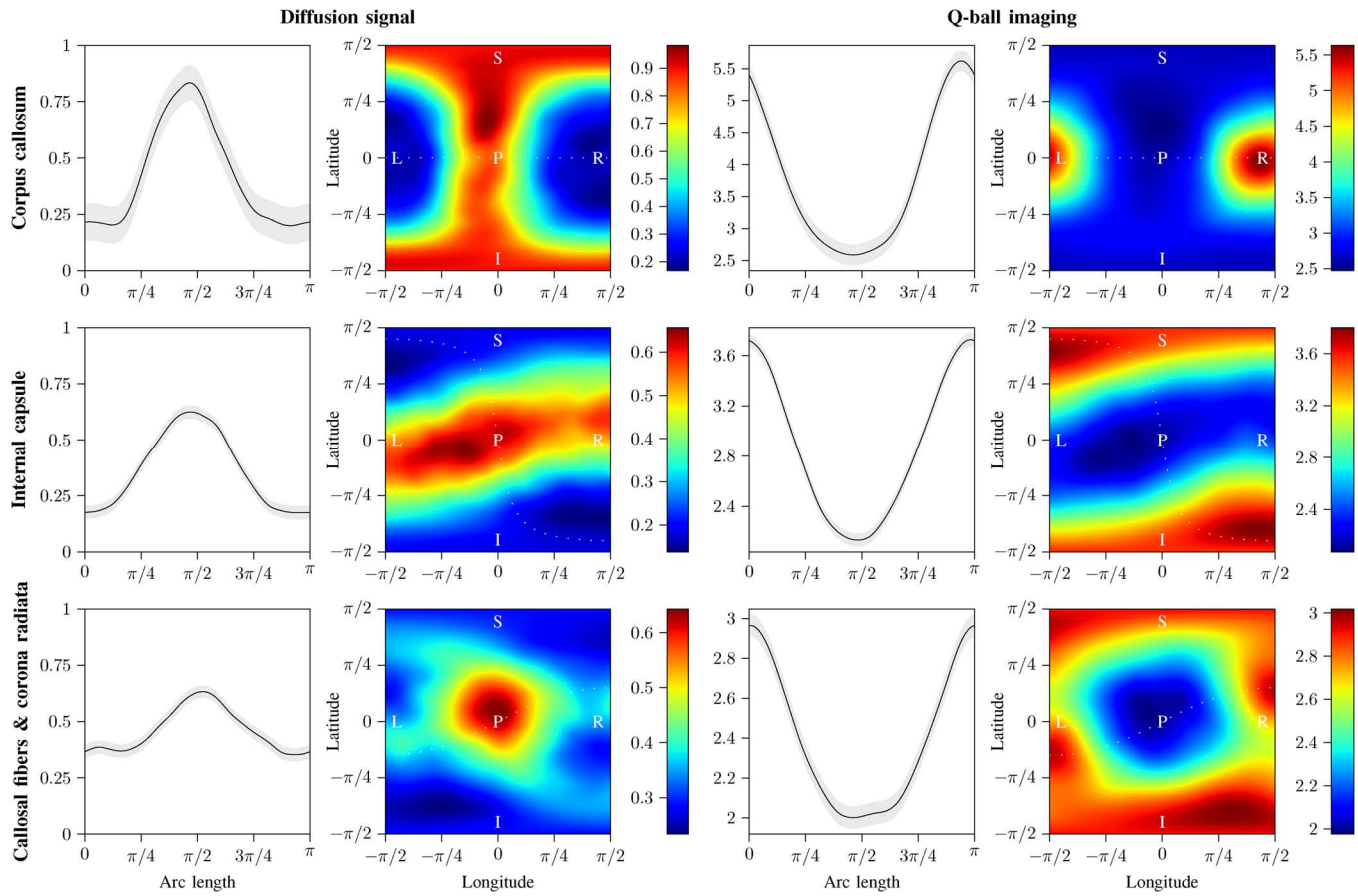

Fig. 4. The estimation of the diffusion signal and the orientation density function (without normalization) is exemplified, from top to bottom, for the three voxels $(0, -35, 15)$, $(-22, -16, 13)$, and $(20, -16, 34)$ in the stereotactic coordinate system [27]. Their fractional anisotropy, T_2-weighted signal, scaling parameter, and noise variance are estimated at $\{0.887, 76.0, 1.54, 136.6\}$, $\{0.694, 242.0, 0.37, 113.6\}$, and $\{0.409, 184.8, 0.26, 92.2\}$, respectively. The first and the third column depict the penalized least squares estimates for a great circle on the sphere, which is shown as dotted line in the second and the fourth column. The shaded area displays the 95% Bayesian confidence band. Abbreviations: left (L), right (R), inferior (I), superior (S), anterior (A), posterior (P).

describing the roughness of the diffusion signal and the noise variance σ^2 of the MR measurement) is an integral part of nonparametric function estimation. In the following simulation study the scaling parameter τ^2 and the noise variance σ^2 are set to 0.5 and 100 in example A, and to 2.0 and 200 in example B, respectively. Note that the former example corresponds to a typical average case, while the latter is rather a worst-case scenario. The factors $w^{(i)}$, which quantify the noise variance modifications due to the linear interpolation, are picked at random from the diffusion dataset. We run 1000 trials to study the estimation of the hyperparameters τ^2 and σ^2 for a finite set of voxels in which these parameters are assumed to be fixed. The spin echo signal in the absence of any diffusion weighting is generated by $E_0 \sim \mathcal{G}\dashv(200/5, 1/5)$ with a mean of 200, which is in the range of the observed T_2-weighted MR signals for white matter. $\mathcal{G}\dashv(\alpha, \beta)$ denotes the Gamma distribution with the density function $f_{\mathcal{G}\dashv}(x; \alpha, \beta) = \beta^\alpha / \Gamma(\alpha) x^{\alpha-1} \exp(-\beta x)$ for $\alpha, \beta > 0$ and $x \in [0, \infty)$. The expectation of $\mathcal{G}\dashv(\alpha, \beta)$ is α/β. The scaling parameter is chosen to be governed by $\mathcal{G}\dashv(30\tau^2, 30)$ with the mean $\tau^2 = 0.5$ in example A and $\tau^2 = 2.0$ in example B, thereby considering that the signal may have various shapes in different voxels. The mean diffusion signal follows $\bar{e}_b \sim \mathcal{G}\dashv(150 \cdot 0.4, 150)$ with the average 0.4, which corresponds to the mean signal typically measured for a b-value of 1500 $\mathrm{s/mm^2}$. Using the acquisition protocol presented earlier, the Gaussian process model simulates the diffusion MR measurements that are disturbed by Rician noise $S^{(i)} \sim \mathcal{R}(E^{(i)}, w^{(i)}\sigma^2)$. The Rician distribution is defined by $f_{\mathcal{R}}(S; E, \varsigma^2) = S/\varsigma^2 \exp(-(S^2 + E^2)/(2\varsigma^2)) I_0(SE/\varsigma^2)$, where S denotes the observed signal, E the true magnitude signal, ς^2 is a parameter characterizing the noise level, and I_0 the zeroth-order modified Bessel function of the first kind. Fig. 2 depicts the sample mean including the 95% confidence interval for the estimation of the scaling parameter $\hat{\tau}^2$ and the noise variance $\hat{\sigma}^2$ with respect to a finite set of voxels. We note that the sample variance rapidly decreases for greater numbers of voxels. Further, in example B there is a slight bias in the estimation of the hyperparameters due to the Rician noise.

B. Data Analysis

Next, we estimate the model parameters $M = \{\tau^2, \sigma^2\}$ that balance the smoothness of the solution against the fidelity to the data. Fig. 3 maps the scaling parameter τ^2 of the prior covariance function and the noise variance σ^2 of the MR measurement in the 26-neighborhood of a voxel. According to the simulation study, the estimation error is expected to be rather small. On the left-hand side of the first and the second row the factors $w^{(i)}$ that quantify the variance modifications due to linear interpolation are neglected. The noise variance, which may be reduced up to 1/8 of the original value, shows wave patterns that are induced by the

correction for subject motion and the alignment with an anatomical coordinate system. In comparison, the right column shows the scaling parameter and the noise variance where the modification factor is taken into account. Higher variance estimates observable in some regions originate from compartments with a high fraction of cerebrospinal fluid or are caused by artifacts due to magnetic susceptibility differences on material interfaces. The scaling parameter, which is much less influenced by the variance modifications, shows significantly higher values in the corpus callosum and the internal capsule, since in these brain regions the diffusion signal is highly anisotropic. The bottom row exemplifies an MR image without any diffusion weighting and the diffusion signal for one of the gradient directions with a b-value of $1500\,\mathrm{s/mm^2}$. Note that this dataset has lower signal intensities in the posterior portion of the brain, which is also visible in the noise variance, but not in the scaling parameter and the diffusion signal, as the T_2-contrast is normalized.

Fig. 4 exemplifies the reconstruction of the diffusion signal and the orientation density function (without normalization) in three voxels taken from different brain regions, namely the corpus callosum, the internal capsule, and the crossing of the callosal fibers with the corona radiata. The first and the third column show the penalized least squares estimates including their 95% Bayesian confidence bands (conditional upon $\boldsymbol{y}$, $\boldsymbol{x}$, $\hat{E}_0$, τ^2, and σ^2) for great circles on the sphere. These bands, which reflect the uncertainty about $\hat{e}_b$ or $\hat{\phi}$ after we have observed the data $\boldsymbol{y}$ at the gradient directions $\boldsymbol{x}$, are given by $\pm\Phi^{-1}(1-\vartheta/2)\sqrt{k_{\mathrm{post}}(\omega,\omega)}$ that specifies the $100(1-\vartheta)\%$ confidence interval at the point $\omega \in S^2$. Φ denotes the cumulative density function of the standard normal distribution and the posterior covariance function k_{post} is formulated in (20) or (29), respectively. The directional functions are shown in polar coordinates and, because these functions are antipodally symmetric, it is sufficient to display them in one hemisphere. For example, the bottom row provides evidence that the fiber population is composed of two fiber bundles, i.e., the crossing of the radiating callosal fibers (from left to right) and the corona radiata (from inferior to superior).

Fig. 5 demonstrates the orientation density field of white matter, which is estimated from a diffusion MR dataset with a b-value of $1500\,\mathrm{s/mm^2}$. The orientation density function ϕ is visualized by the quasi-spherical surface $S^2 \ni \omega \mapsto \phi(\omega)\omega \in \mathbb{R}^3$. Red denotes a left-right orientation, green an anterior-posterior direction, and blue a superior-inferior orientation. It is common practice that the minimum of the orientation density function is subtracted, but we do not normalize with respect to the maximum value. The underlying map shows the fractional anisotropy provided by the diffusion tensor model. Recall that the callosal fibers (cc) are commissural fibers which interconnect the two hemispheres, whereas the corona radiata (cr) includes, for instance, the pyramidal tract which is a projection fiber bundle primarily linking the motor cortex with the spinal cord. The figure uncovers the intermingling of these two nerve fiber systems in the coronal plane.

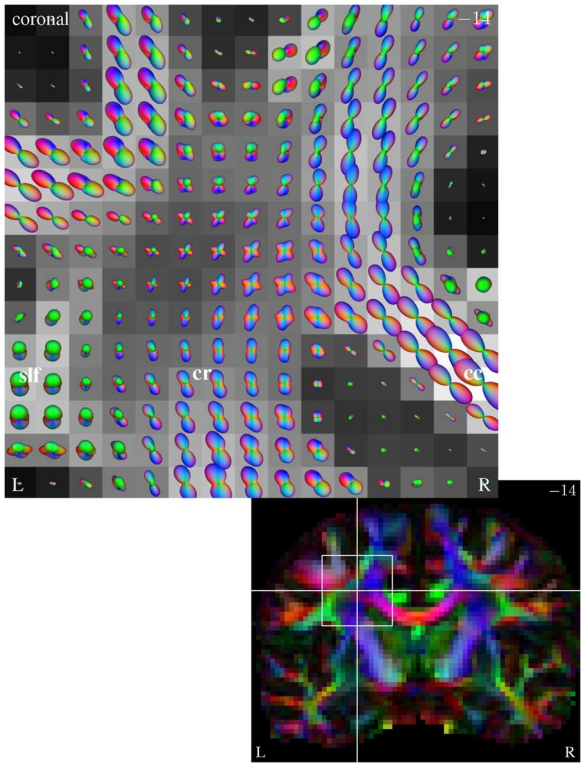

Fig. 5. The orientation density field exposes the radiation of the corpus callosum (cc), the corona radiata (cr), and their crossing. The underlying map depicts the fractional anisotropy. The number in the upper right corner indicates the coronal slice in the anatomical coordinate system [27]. Abbreviation: superior longitudinal fasciculus (slf).

IV. Discussion

Q-ball imaging is widely used nowadays to exploit the directional dependence of the water diffusion process to uncover the fiber architecture in the human brain white matter. This method is based on the narrow pulse assumption and a Stejskal–Tanner experiment [28], which consists of two diffusion sensitizing gradient pulses with infinitesimally short duration but finite diffusion weighting. This approximation allows to establish a Fourier relationship between the diffusion propagator and the observable MR signal. However, short gradient pulses with high intensity are difficult to achieve in human subjects due to safety concerns. Diffusion encoding gradients are switched on for a considerable time and hence the diffusion process during the application of the gradient fields may not be negligible. Under the narrow pulse assumption, Tuch [3] argues that the orientation density function of the diffusion propagator and the Funk–Radon transform of the diffusion signal differ in a term including a zeroth-order Bessel function of the first kind, which exhibits high oscillations. If the timing of the MR sequence is kept fixed, we expect that the orientation density function of the diffusion propagator is invariant with respect to the strength of the diffusion encoding gradients. However, the Funk–Radon transform of the observed signal depends not only on the diffusion process as suggested by Q-ball imaging, but also on the gradient magnitude. Although the diffusion propagator is the same in this experimental setting, the *effective* or *apparent* orientation density function is varying.

Generally, the (local) maxima of the orientation density function of the diffusion propagator do not agree with the number of fiber bundles and their orientation. Note that even the modes of the fiber orientation density generally do not correspond to the respective directions of the fiber subpopulations [29]. Consider a mixture of two univariate Gaussian distributions. Depending

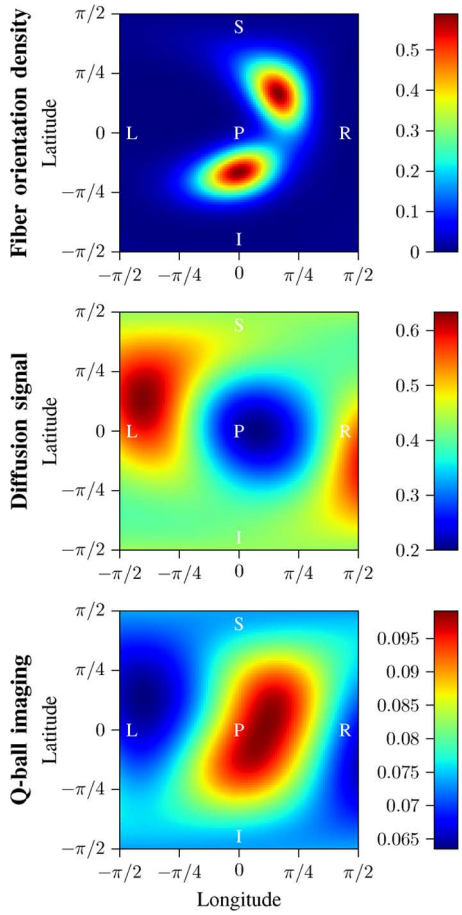

Fig. 6. The fiber orientation distribution (top) is convolved with the impulse response of a fiber segment, yielding the diffusion signal shown in the middle row. The orientation density function as defined by Q-ball imaging (with normalization, bottom) is obtained from the Funk–Radon transform of the diffusion signal.

on their mean and variance, there may be either one or two maxima, which in most cases do not agree with the respective means of the two normal densities. Obviously, this argument generalizes to fiber populations composed of two or more fiber bundles. Provided that noise artifacts are negligible, a better interpretation might be that the number of modes is a lower bound for the number of fiber bundles. Although there are many examples with a good agreement (especially for voxels with one fiber bundle), we cannot be sure whether the fiber population is accurately reflected by the orientation density function, as shown in simulations [30] and in a phantom study [31]. Another example is given in Fig. 6. Assume that the impulse response of a fiber segment is described by the diffusion tensor model with the water diffusivity parameters $\lambda_1 = 0.0018\ \mathrm{mm}^2/\mathrm{s}$ parallel to a nerve fiber and $\lambda_2 = 0.0002\ \mathrm{mm}^2$ perpendicular to it. The spherical convolution with the fiber orientation distribution which consists of two fiber subpopulations represented by a mixture of two Bingham distributions (with an angular separation of 66.5° [29]) yields for a b-value of 1500 $\mathrm{s/mm}^2$ the diffusion signal displayed in the middle row. It is apparent that the Funk–Radon transform of the signal, which is depicted with normalization in the bottom section of this figure, does not show close similarity with the fiber orientation distribution (top). The latter can be recovered from diffusion-weighted

Algorithm 1: Computation of the orientation density function (ODF).

Input: n diffusion MR measurements $y^{(i)}$ and variance modifications $w^{(i)}$ at each site s for the corresponding gradient directions $g^{(i)}$;
Output: estimate of the ODF $\hat{\phi}(\omega)$ at each site s;
compute the n-vector J with the entries $(Y_{0,0})_i$ using (3);
compute the $n \times n$-matrix K with the elements $(\zeta^1(g^{(i)}, g^{(j)}))_{i,j}$ using (10);
compute the QR decomposition $J = (Q_1\ Q_2)(R^t\ 0^t)^t$ with the $n \times 1$-matrix Q_1, the $n \times (n-1)$-matrix Q_2, and the upper triangular 1×1-matrix R;
for *each site* s **do**
  estimate the sample mean $\hat{E}_0$ at s;
  compute the n-dimensional diagonal matrix W with the entries $(w^{(i)})_{i,i}$ at s;
  estimate the regularization parameter ξ in the 26-neighborhood of s (cf. Section II-A);
  $\boldsymbol{\beta} = Q_2(Q_2^t[K + \xi/\hat{E}_0^2 W]Q_2)^{-1}Q_2^t \boldsymbol{y}/\hat{E}_0$;
  $\alpha = R^{-1}Q_1^t(\boldsymbol{y}/\hat{E}_0 - [K + \xi/\hat{E}_0^2 W]\boldsymbol{\beta})$;
  estimate the ODF $\hat{\phi}(\omega)$ at s using (28);
end

MR measurements by using spherical deconvolution techniques [32], [33], for instance, a maximum entropy method [34], the parametric description of the fiber population via a finite mixture of Bingham distributions [29], or the nonparametric representation of the fiber orientation density in a reproducing kernel Hilbert space [35].

In conclusion, Q-ball imaging computes a summary statistics of the diffusion propagator, namely the apparent orientation density function. This technique relies on the nonparametric function estimation of the diffusion signal. We propose to solve the variational problem in a reproducing kernel Hilbert space, which is dense in the infinite-dimensional space of the real-valued antipodally symmetric square-integrable functions on the sphere. Previous approaches [11]–[13] are special cases, since these methods truncate the spherical harmonic expansion, assuming that in the observed signal the harmonic coefficients greater than a specified order are zero. This assumption is weakened here, so that these coefficients decay sufficiently fast, which may reduce ringing and blurring artifacts. The corresponding Gaussian process model allows the rigorous voxel-by-voxel estimation of the hyperparameters, which are the roughness of the diffusion signal and the noise variance of the MR measurement. Note that the noise in the magnitude of the complex-valued signal is well approximated by a Gaussian distribution for relatively low b-values and sufficiently high signal-to-noise ratios. If the diffusion dataset does not meet these experimental conditions, a Rician noise model might be considered [36]. Our novel approach is easy to implement and does not require user-defined parameters, which are estimated from the data or, if possible, are avoided completely. Thus, Q-ball imaging is particularly valuable in clinical environments, also due to the short acquisition time.

ACKNOWLEDGMENT

The diffusion-weighted MR dataset analyzed in the present study was kindly provided by the 2009 Pittsburgh Brain Connectivity Competition [24].

REFERENCES

[1] D. Le Bihan, "Looking into the functional architecture of the brain with diffusion MRI," *Nature Rev. Neurosci.*, vol. 4, pp. 469–480, 2003.
[2] C. Beaulieu, "The basis of anisotropic water diffusion in the nervous system—A technical review," *NMR Biomed.*, vol. 15, pp. 435–455, 2002.
[3] D. S. Tuch, "Q-ball imaging," *Magn. Reson. Med.*, vol. 52, pp. 1358–1372, 2004.
[4] E. J. Canales-Rodríguez, L. Melie-García, and Y. Iturria-Medina, "Mathematical description of q-space in spherical coordinates: Exact q-ball imaging," *Magn. Reson. Med.*, vol. 61, pp. 1350–1367, 2009.
[5] A. Tristán-Vega, C.-F. Westin, and S. Aja-Fernández, "Estimation of fiber orientation probability density functions in high angular resolution diffusion imaging," *NeuroImage*, vol. 47, pp. 638–650, 2009.
[6] I. Aganj, C. Lenglet, G. Sapiro, E. Yacoub, K. Ugurbil, and N. Harel, "Reconstruction of the orientation distribution function in single- and multiple-shell q-ball imaging within constant solid angle," *Magn. Reson. Med.*, vol. 64, pp. 554–566, 2010.
[7] A. Tristán-Vega, C.-F. Westin, and S. Aja-Fernández, "A new methodology for the estimation of fiber populations in the white matter of the brain with the Funk-Radon transform," *NeuroImage*, vol. 49, pp. 1301–1315, 2010.
[8] M. H. Khachaturian, J. J. Wisco, and D. S. Tuch, "Boosting the sampling efficiency of q-ball imaging using multiple wavevector fusion," *Magn. Reson. Med.*, vol. 57, pp. 289–296, 2007.
[9] R. Deriche, J. Calder, and M. Descoteaux, "Optimal real-time q-ball imaging using regularized Kalman filtering with incremental orientation sets," *Med. Image Anal.*, vol. 13, pp. 564–579, 2009.
[10] K. K. Seunarine and D. C. Alexander, "Multiple fibers: Beyond the diffusion tensor," in *Diffusion MRI: From Quantitative Measurement to In-Vivo Neuroanatomy*. New York: Elsevier, 2009, pp. 55–72.
[11] A. W. Anderson, "Measurement of fiber orientation distributions using high angular resolution diffusion imaging," *Magn. Reson. Med.*, vol. 54, pp. 1194–1206, 2005.
[12] C. P. Hess, P. Mukherjee, E. T. Han, D. Xu, and D. B. Vigneron, "Q-ball reconstruction of multimodal fiber orientations using the spherical harmonic basis," *Magn. Reson. Med.*, vol. 56, pp. 104–117, 2006.
[13] M. Descoteaux, E. Angelino, S. Fitzgibbons, and R. Deriche, "Regularized, fast, and robust analytical q-ball imaging," *Magn. Reson. Med.*, vol. 58, pp. 497–510, 2007.
[14] G. K. Rohde, A. S. Barnett, P. J. Basser, and C. Pierpaoli, "Estimating intensity variance due to noise in registered images: Applications to diffusion tensor MRI," *NeuroImage*, vol. 26, pp. 673–684, 2005.
[15] G. Wahba, "Spline interpolation and smoothing on the sphere," *SIAM J. Sci. Stat. Comput.*, vol. 2, pp. 5–16, 1981.
[16] G. Sansone, *Orthogonal Functions*. Mineola, NY: Dover, 2004.
[17] N. Aronszajn, "Theory of reproducing kernels," *Trans. Am. Math. Soc.*, vol. 68, pp. 337–404, 1950.
[18] J. Gustavsson, "Some sums of Legendre and Jacobi polynomials," *Mathematica Bohemica*, vol. 126, pp. 141–149, 2001.
[19] G. Kimeldorf and G. Wahba, "Some results on Tchebycheffian spline functions," *J. Math. Anal. Appl.*, vol. 33, pp. 82–95, 1971.
[20] G. Kimeldorf and G. Wahba, "A correspondence between Bayesian estimation of stochastic processes and smoothing by splines," *Ann. Math. Stat.*, vol. 41, pp. 495–502, 1970.
[21] D. V. Lindley and A. F. M. Smith, "Bayes estimates for the linear model," *J. R. Stat. Soc.: Ser.B*, vol. 34, pp. 1–41, 1972.
[22] A. O'Hagan, "Curve fitting and optimal design for prediction," *J. R. Stat. Soc.: Ser. B*, vol. 40, pp. 1–42, 1978.
[23] C. F. Ansley and R. Kohn, "Estimation, filtering, and smoothing in state space models with incompletely specified initial conditions," *Ann. Stat.*, vol. 13, pp. 1286–1316, 1985.
[24] W. Schneider, "Pittsburgh brain connectivity competition 2009: Mapping the human connectome," in *Proc. 15th Annu. Meeting Organizat. Human Brain Mapp.*, 2009, p. S28.
[25] M. Jenkinson, P. Bannister, M. Brady, and S. Smith, "Improved optimization for the robust and accurate linear registration and motion correction of brain images," *NeuroImage*, vol. 17, pp. 825–841, 2002.
[26] FMRIB Software Library 4.1 Univ. Oxford, 2008 [Online]. Available: http://www.fmrib.ox.ac.uk/fsl
[27] J. Talairach and P. Tournoux, *Co-Planar Stereotaxic Atlas of the Human Brain*. New York: Thieme, 1988.
[28] E. O. Stejskal and J. E. Tanner, "Spin diffusion measurements: Spin echoes in the presence of a time-dependent field gradient," *J. Chem. Phys.*, vol. 42, pp. 288–292, 1965.
[29] E. Kaden, T. R. Knösche, and A. Anwander, "Parametric spherical deconvolution: Inferring anatomical connectivity using diffusion MR imaging," *NeuroImage*, vol. 37, pp. 474–488, 2007.
[30] W. Zhan and Y. Yang, "How accurately can the diffusion profiles indicate multiple fiber orientations? A study on general fiber crossings in diffusion MRI," *J. Magn. Reson.*, vol. 183, pp. 193–202, 2006.
[31] J.-D. Tournier, C.-H. Yeh, F. Calamante, K.-H. Cho, A. Connelly, and C.-P. Lin, "Resolving crossing fibres using constrained spherical deconvolution: Validation using diffusion-weighted imaging phantom data," *NeuroImage*, vol. 42, pp. 617–625, 2008.
[32] E. A. H. von dem Hagen and R. M. Henkelman, "Orientational diffusion reflects fiber structure within a voxel," *Magn. Reson. Med.*, vol. 48, pp. 454–459, 2002.
[33] J.-D. Tournier, F. Calamante, D. G. Gadian, and A. Connelly, "Direct estimation of the fiber orientation density function from diffusion-weighted MRI data using spherical deconvolution," *NeuroImage*, vol. 23, pp. 1176–1185, 2004.
[34] D. C. Alexander, "Maximum entropy spherical deconvolution for diffusion MRI," in *Proc. 19th Int. Conf. Inf. Process. Med. Imag.*, 2005, pp. 76–87.
[35] E. Kaden, A. Anwander, and T. R. Knösche, "Variational inference of the fiber orientation density using diffusion MR imaging," *NeuroImage*, vol. 42, pp. 1366–1380, 2008.
[36] R. A. Clarke, P. Scifo, G. Rizzo, F. Dell'Acqua, G. Scotti, and F. Fazio, "Noise correction on Rician distributed data for fibre orientation estimators," *IEEE Trans. Med. Imag.*, vol. 27, no. 9, pp. 1242–1251, Sep. 2008.